Virtual-point-based geometric error compensation model for additive manufacturing machines

Pablo Zapico, Fernando Peña, Gonzalo Valiño, José Carlos Rico, Víctor Meana, Sabino Mateos

Department of Construction and Manufacturing Engineering, University of Oviedo, Oviedo, Spain

Abstract

Purpose: The lack of geometric and dimensional accuracy of parts produced by additive manufacturing (AM) is directly related to the machine, material and process used. This work proposes a method for the analysis and compensation of machine-related geometric errors applicable to any AM machine, regardless of the manufacturing process and technology used.

Design/methodology/approach: For this purpose, an error calculation model inspired by those used in CNC machines and CMMs was developed. The error functions of the model were determined from the position deviations of a set of virtual points that are not sensitive to material and process errors. These points were obtained from the measurement of an ad hoc designed and manufactured master artefact. To validate the model, off-line compensation was applied to both the original designed artefact and an example part.

Findings: The geometric deviations in both cases were significantly smaller than those found before applying the geometric compensation. Dimensional enhancements were also achieved on the example part by using a correction parameter available in the 3D printing software, whose value was adjusted from the measurement of the geometrically compensated master artefact.

Research limitations/implications: The errors that persist in the part derive from both material and process. Compensation for these type of errors requires a detailed analysis of the influencing parameters, which will be the subject of future research.

Originality/value: The use of the virtual-point-based error model increases the quality of additively manufactured parts and can be used in any AM system.

Keywords: Additive Manufacturing, Geometric error compensation, Machine error model, Virtual point.

1. Introduction

A remarkable evolution has taken place from rapid prototyping (RP) techniques born in the 1980s to today's additive manufacturing (AM) processes. This progress has had impact from prototyping to obtaining fully functional, highly complex parts in a wide variety of materials, with a customised design and without a significant cost increase (Campbell *et al.*, 2012; ISO, 2015). For this reason, AM techniques have attracted particular interest in leading sectors such as medical, aerospace, automotive, military, etc. (Javaid and Haleem, 2018; Najmon *et al.*, 2019). However, the lack of specific consolidated regulations, as well as the low quality of parts obtained in certain cases, still greatly limit their industrial applicability (Moroni *et al.*, 2020).

A relevant aspect to measure the quality of mechanical components has to do with their geometric and dimensional accuracy in combination with their surface finish

characteristics. In parts obtained by AM, the lack of geometric and dimensional accuracy derives mainly from three possible error sources (Abdelrahman *et al.*, 2017; Hartmann *et al.*, 2019; Vanaei *et al.*, 2020; Omairi *et al.*, 2021):

- Process parameters: although process parameters greatly depend on the characteristics of the AM technology considered (ISO, 2015), some of them are common to almost all processes and materials, such as layer thickness, consolidation zone width, hatch distance, infill density, scanning strategy, scanning velocity or even the amount of energy necessary to prepare and transform the material (Sood *et al.*, 2009; Foster *et al.*, 2015; Fang *et al.*, 2017; Klassen *et al.*, 2017; Elkaseer *et al.*, 2020; Oliveira *et al.*, 2020; Haghshenas Gorgani *et al.*, 2021; Mohamed *et al.*, 2021).
- Material properties: although they also depend partially on the considered technology, some properties affect to most of the processes, such as density, surface tension, thermal conductivity, moisture absorption or melting temperature (Sutton *et al.* 2016; Vock *et al.* 2019; Yuasa *et al.* 2021; Fico *et al.* 2022; Shanmugam *et al.* 2021).
- Machine errors: regardless of the considered technology, constructive components (hardware and software) of the AM machines cause kinematic errors, loads, dynamics forces and control errors that are transferred to the part under construction (ISO, 2012; Bochmann *et al.*, 2015; Cajal *et al.*, 2016; Lyu & Manoochehri, 2019; Tong *et al.*, 2003, 2008).

These three error sources simultaneously affect the quality of the manufactured part, with machine-related errors being essentially systematic. Knowing the specific contribution of machine errors would make it possible to compensate for those of a systematic nature and to be able to analyse which parameters related to the process and the material are more relevant to improve the part quality. Furthermore, the compensation of machine errors will favour the reproducibility of the results achieved in the characterisation of process errors in different machines, an aspect that unfortunately is not valued in many of the works that have been developed in this context so far.

Procedures used for geometric errors characterisation of CNC machines are well stablished and can be classified into direct and indirect methods (Schwenke *et al.*, 2008). The former are aimed at characterising each error individually, while the latter characterise several errors simultaneously. Both methods can be based on the use of artefacts (Carmignato *et al.*, 2020) as well as highly accurate measurement systems (Deng *et al.*, 2020). In the case of production machines, which do not usually have integrated part measurement systems, it is common to carry out indirect methods that consist of manufacturing an artefact on the machine and then measuring it on a CMM (Schellekens *et al.*, 1993). This error measurement technique is also the most widely used in AM machines. A proof of this are some works previously developed by different researchers (Tong *et al.*, 2003, 2008; Bochmann *et al.*, 2015; Song *et al.*, 2014; Cajal *et al.*, 2016; Majarena *et al.*, 2017; Lyu *et al.*, 2017), as well as the proposal of the ISO/ASTM 52902 standard to assess the geometric capacity of AM systems using artefacts.

However, the previous studies do not isolate the different error sources, so their results are limited to the particular machines and AM techniques considered in each case. Therefore, it becomes important to develop procedures to characterise and compensate for the geometric errors of AM machines while avoiding the influence of the process and material-related errors.

The use of external systems that simulate the behaviour of the machine to compensate for

its geometric errors has become a common technique. For instance, the use of *Digital Twins* (DT), successfully applied in many fields related to Industry 4.0 (Tao *et al.*, 2019; Leng *et al.*, 2021), makes it possible by using a twin virtual machine (Kadir *et al.*, 2011; Iñigo *et al.*, 2021). However, in the case of AM it is most common to use mathematical computer models to predict machine errors and compensate for them by one of the following procedures:

- Modifying the original design of the part (Lyu *et al.*, 2017; Beltrán *et al.*, 2021).
- Modifying the STL model of the part (Wang *et al.*, 2008; Cajal *et al.*, 2016).
- Correcting the G-code that will be run on the machine control (Tong *et al.*, 2008; Majarena *et al.*, 2017).

Among these methods, the first two are the most recommendable as they allow for the tool path compensation, and not only for the target positions reached by the forming element during manufacture. Since the geometry included in the STL file consists of triangles, its modification only involves the correction of the triangle vertices and their normal vectors (Tong *et al.*, 2004) avoiding the need for complicated geometric transformations in the original CAD model (Beltrán *et al.*, 2021).

Taking into account the previous considerations, the present study develops a model for prediction and off-line compensation for geometric errors of AM machines. The model is based on polynomial expressions whose coefficients are calculated from the measurement of a master artefact designed ad hoc and manufactured in an AM test bench. Among the most innovative aspects of this model compared to those of other authors, the following stand out:

- The metrological information of the artefact designed is based on the calculation of virtual points, which makes it possible to isolate to a large extent the geometric errors of the machine from the process and material-related errors. As a consequence, although the model was developed on the basis of an FFF machine, the methodology is applicable to any other type of AM machine. In contrast, the methodologies applied in other works do not consider the separation of the different error sources and are therefore less effective for different combinations of machine, process and material.
- As in other works, a kinematic model that takes into account the different moving parts of the AM machine was developed. However, unlike them, this model has been adapted to the particular characteristics of AM machines by eliminating some error functions that can cause problems in the operation of the machine and in the quality of the manufactured parts (see section 3.2). In addition, this made it possible to simplify the model, with all the advantages that this entails.
- Polynomial error functions were used in the developed model and their coefficients were calculated using the least squares method. In the validation of the method, low statistical significance of some of these coefficients was observed, which allowed for an additional simplification of the model (see section 3.2). In some works, the relevance of these coefficients is not studied, which can lead to overfitting and a higher computational cost, whereas in others, the coefficients are calculated by iterative methods that do not ensure an optimal solution, resulting in a local minimum of the residuals.

To validate the developed error model, off-line compensation was applied to the STL file of the original artefact, and it was metrologically verified that the newly manufactured artefact had got significantly smaller geometrical deviations than the original. This

predictive error model was also applied to the manufacture of an example part where, in addition to the compensation of geometric errors, dimensional accuracy of the functional features was improved too.

2. Experimental equipment

2.1. Test bench

A test bench of our own design was used to analyse the developed geometric error compensation model. This is a kind of AM machine based on FFF (Peña *et al.*, 2021). The test bench has got a ZFXY−axis architecture (Zhang, 2012) consisting of a fixed structure (F), with respect to which a build platform moves along the vertical direction (Z axis), as well as an extrusion head fixed to a carriage movable along the Extrusion bridge (Y direction). This bridge can also be displaced along X direction on the frame. Synchronization of movements on both axes makes it possible the tracing of 2D paths in the horizontal plane to deposit each material layer (Figure 1). The test bench working volume is $280 \times 280 \times 280$ mm^3, enabling layer height values between 0.06 and 0.60 mm and using a nozzle of 0.4 mm diameter. The material used in the tests was grey PLA thermoplastic with a diameter of 2.85 mm.

NEMA stepper motors are used to drive X, Y, Z axes with resolution of 5 µm on each axis. The test bench is controlled by an MKS Rumba motherboard running Marlin Firmware 1.1.9, an AM machine-specific firmware. The 3D printing software used to generate the G-code of parts to be manufactured is Ultimaker Cura 4.8.0.

Although an inspection bridge is shown in Figure 1, this system is not used in this work and thus it will not be described in detail.

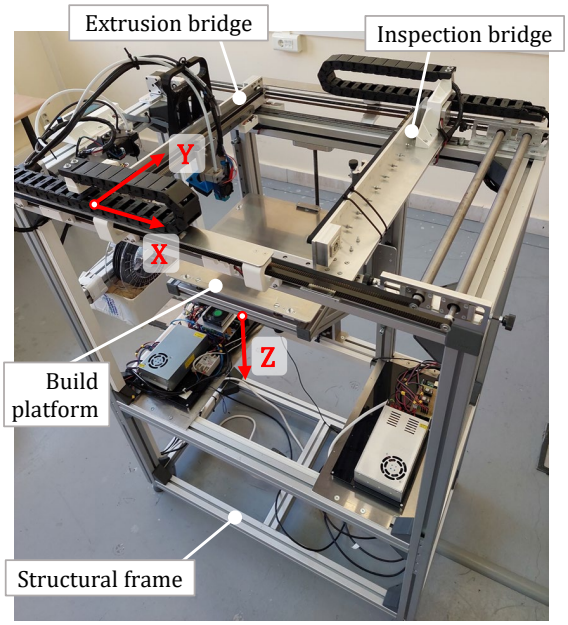

Figure 1. Test bench for 3D printing based on FFF.

2.2. Coordinate Measuring Machine

Measurements of the artefact and manufactured parts on the test bench were performed on a DEA Global Image Coordinate Measuring Machine (CMM) equipped with a motorized indexable head Renishaw PH10-MQ and a SP25M scanning probe system. A 30 mm long ceramic stylus tip with a 3 mm diameter ruby ball was used in this work.

Hexagon PC-DMIS 2015.1 was used as inspection software. The metrological performance of this CMM, maximum repeatability specified value and maximum permissible error for linear measurements, are respectively (ISO, 2009):

$$R_{0,MPL} = 2.2\ \mu m \tag{1}$$

$$E_{0,MPE} = 2.2 + 3L \cdot 10^{-3}\ \mu m, \text{being } L \text{ in mm} \tag{2}$$

2.3. Artefact for the adjustment of the machine errors model

In order to characterise the geometric errors of a machine, it is usual to design a specific artefact which, once manufactured, can be measured to extract the metrological information (distances, orientations, position of control points, etc.) to deduce deviations from its theoretical geometry. Since this work is intended to characterise only the geometric errors of the machine, the artefact shall be designed to minimise the influence of the material and process on the measured errors.

In FFF, process and material-related dimensional and geometric variations occur mainly in the X and Y directions, resulting from several factors, among which the most important are the cross-section of the filament deposited during the building of each layer and the volumetric shrinkage that the material undergoes when cooling from the time it is deposited in the layer until room temperature is reached.

On the one hand, the cross-section of the filament is circular and coincides with the cross-section of the nozzle just as it passes through, but becomes wider than high as it is deposited on the layer. This is because the layer height is always smaller than the nozzle diameter (usually in proportion 1/2 or 1/4) and, by conservation of mass, the filament width will be larger, in a proportion that will also depend on the ratio between the flow velocity through the nozzle and the nozzle displacement velocity in the material deposition (Moretti, 2021).

As far as volumetric shrinkage is concerned, the possible variation that may occur in the vertical direction will be compensated for because the height of each layer is set by the machine control when positioning the nozzle in the Z-axis. Therefore, this effect will influence more importantly in X and Y directions.

Thus, to reduce the effect of process errors, the artefact shall be designed to provide metrological information that is low sensitive to deformation taking place mainly in the horizontal plane.

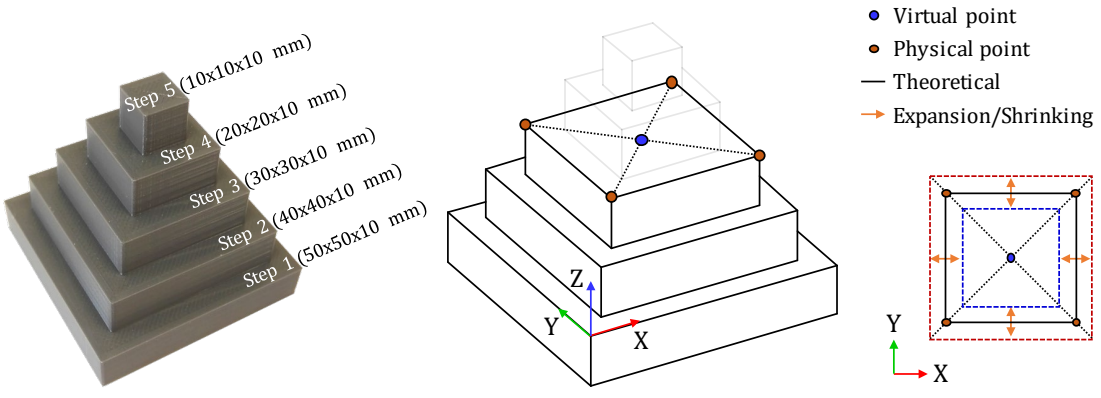

(a) (b)

Figure 2. (a) Stepped pyramid of the master artefact, (b) Representation of a virtual point on the third step.

For this purpose, it is suggested to use an artefact based on stepped pyramids as shown in Figure 2a. This geometry will allow metrological information to be extracted from different control positions consisting of virtual points located at the centre of the upper surface of each step of the pyramid (Figure 2b). For each step, the positions of the virtual points are obtained by geometric operations between the planes of its four vertical faces and its horizontal faces. Although the effects of dimensional and geometrical deviations derived from the AM process could cause a variation in the distance between the vertical faces parallel to each other, the location of the virtual points calculated does not change (Figure 2b). In other words, the virtual points are not affected by the possible deformations that the material may suffer in the horizontal plane as a result of the process.

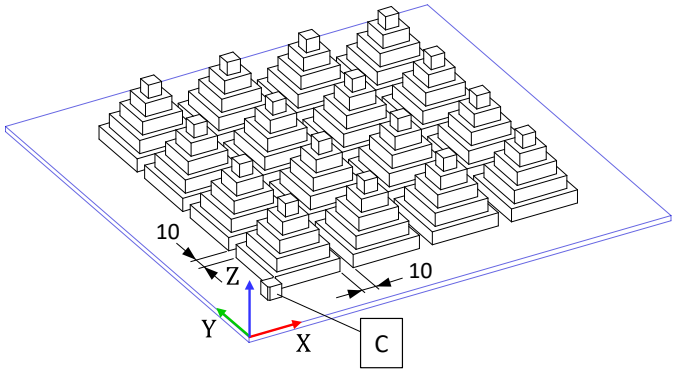

Figure 3. Master artefact consisting of 16 pyramids.

Using a set of these pyramids distributed over the build platform of the AM machine, it will be possible to obtain a 3D distribution of control points associated with different positions in its working space. The dimensions, quantity and distribution of the pyramids must be adapted to the working space of the machine and will determine the number of control points.

In this work, 16 pyramids built with a layer thickness of 0.10 mm and spaced 10 mm from each other were used, as shown in Figure 3. The cube C was employed to align the artefact in the CMM. With this artefact 80 control points (5 points per pyramid) and 160 distances (10 distances per pyramid) measured between the vertical planes of the steps of the different pyramids can be obtained.

Once designed the artefact, it was manufactured on the test bench using the FFF process parameters shown in Table 1.

Table 1. Parameters used for manufacturing the artefact (Ultimaker Cura).

Parameter	Value
Layer height (mm)	0.10
Wall thickness (mm)	1.60
Top/Bottom thickness (mm)	0.80
Infill density (%)	8
Infill pattern	Grid
Extruder temperature (°C)	190
Build plate temperature (°C)	58

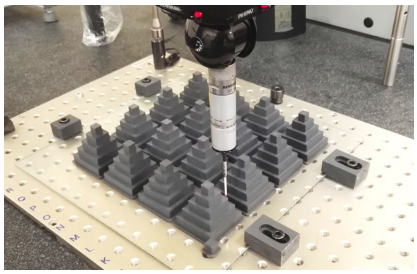

(a)

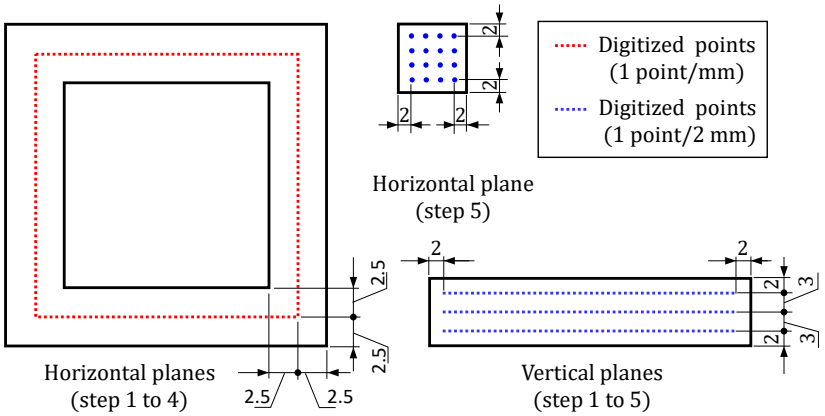

(b)

Figure 4. Artefact measurement on the CMM: (a) set-up, (b) points distribution on each pyramid plane.

After manufacturing, the artefact was measured on the CMM. According to ISO/ASTM 52902, to avoid distortions of the artefact when removing it from the test bench that could affect the measurement results, the artefact was placed on the CMM together with the glass of the build platform (Figure 4a). Next, all the horizontal and vertical planes of the pyramids were digitised according to the layout and density of points shown in Figure 4b.

Through the measurement process, 50,000 points were obtained to adjust the different horizontal and vertical planes of the pyramids and to determine the physical and virtual points as shown in Figure 2b. For each step, the virtual points associated with the upper and lower planes were determined, except for the first step, where only the virtual point associated with the upper plane could be obtained. In this way, two different virtual points were determined in the planes located between two consecutive steps. In summary, 9 virtual points were obtained in each pyramid and 144 in the whole artefact.

3. Machine error model

3.1. General model

During parts manufacturing on the test bench, relative displacements of the different components occur along the axes of movement. If these components are considered as quasi-rigid bodies, reference systems associated to each of them can be defined (Figure 5a) including one associated to the machine frame:

- (OXYZ) − Build platform
- ($O_1X_1Y_1Z_1$) − Frame
- ($O_2X_2Y_2Z_2$) − Extrusion bridge
- ($O_3X_3Y_3Z_3$) – Carriage

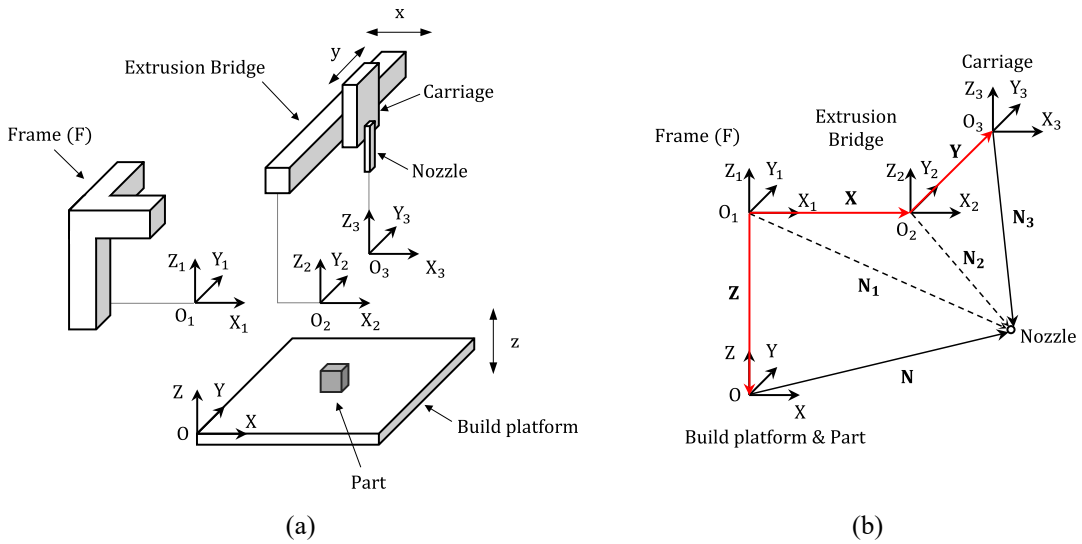

Figure 5. Kinematic chain of the AM machine: (a) axes diagram, (b) axes reference systems.

These reference systems coincide in position and orientation at the machine zero point. The objective of the geometric error model is to determine the nozzle position expressed in the reference system of the build platform (**N**) considering the kinematic imperfections and geometric errors of the machine (Figure 5b). For this, it is necessary to define these errors and to traverse the kinematic chain linking this reference system to the nozzle.

The position and space orientation of each of the quasi-rigid bodies involved in this kinematic chain is defined by 6 degrees of freedom: 3 displacements and 3 rotations. These degrees of freedom can be used to model the kinematic errors of each of the moving components of the machine: build platform, bridge and carriage. This gives the displacement and angular errors included in Table 2, which represent errors concerning the 6 degrees of freedom in the movements of each moving component, due to displacements of the x, y and z machine axes. Considering that the movement of several axes is combined, a squareness error must be added to the above errors for each pair of axes involved. These squareness errors are constants representing the lack of perpendicularity of the motion directions of the different quasi-rigid bodies considered, and can be defined differently depending on the machine axis used as a reference (Kruth, 1994).

Table 2. Error functions of the AM machine moving components.

	Machine component and displacement axis		
	Build platform z	Extrusion bridge x	Carriage y
Displacement error			
Linear	$\delta_z(z)$	$\delta_x(x)$	$\delta_y(y)$
Straightness	$\delta_z(x), \delta_z(y)$	$\delta_x(z), \delta_x(y)$	$\delta_y(z), \delta_y(x)$
Angular error			
Roll	$\varepsilon_z(z)$	$\varepsilon_x(x)$	$\varepsilon_y(y)$
Pitch	$\varepsilon_x(z)$	$\varepsilon_y(x)$	$\varepsilon_x(y)$
Yaw	$\varepsilon_y(z)$	$\varepsilon_z(x)$	$\varepsilon_z(y)$
Squareness error	α_{xz}, α_{yz}	-	α_{xy}

Once these errors have been defined, to traverse the kinematic chain linking the part to the nozzle tip, it is necessary to perform the transformations between the different reference systems from OXYZ to $O_3X_3Y_3Z_3$ (Figure 5a). The displacements of the build platform, bridge and carriage, as a function of the machine axes z, x, y, are represented by the vectors Z, X, Y shown in Figure 5b, and can be calculated as follows:

$$\mathbf{Z} = \begin{pmatrix} -\delta_x(z) + z \cdot \alpha_{xz} \\ -\delta_y(z) + z \cdot \alpha_{yz} \\ -(z + \delta_z(z)) \end{pmatrix}; \ \mathbf{X} = \begin{pmatrix} x + \delta_x(x) \\ \delta_y(x) \\ \delta_z(x) \end{pmatrix}; \ \mathbf{Y} = \begin{pmatrix} \delta_x(y) - y \cdot \alpha_{xy} \\ y + \delta_y(y) \\ \delta_z(y) \end{pmatrix} \quad (3)$$

These vectors, added to the position of the nozzle tip expressed in the carriage reference system ($\mathbf{N_3}$) are not sufficient to define the position of the nozzle in the part reference system, since they are expressed in different reference systems: $\mathbf{Z}$ and $\mathbf{X}$ are expressed in the frame reference system ($O_1X_1Y_1Z_1$) and $\mathbf{Y}$ in the extrusion bridge system ($O_2X_2Y_2Z_2$). To perform the transformation of these vectors along the kinematic chain, from one axis system to the next, rotation matrices shall be used, which can be represented in a simplified form according to equation (4) and provided that the expected geometric errors are small (Zhang, 2012).

$$R(a) = \begin{pmatrix} 1 & \varepsilon_z(a) & -\varepsilon_y(a) \\ -\varepsilon_z(a) & 1 & \varepsilon_x(a) \\ \varepsilon_y(a) & -\varepsilon_x(a) & 1 \end{pmatrix} \quad (4)$$

where a can take the values x, y or z. Accordingly, the position of the nozzle expressed in the Frame, Extrusion Bridge and Carriage systems ($\mathbf{N_1}, \mathbf{N_2}, \mathbf{N_3}$, respectively) are obtained by means of equations (5) to (6), as shown in Figure 5b.

$$\mathbf{N} = R(z)\{\mathbf{N_1} - \mathbf{Z}\} \quad (5)$$

$$\mathbf{N_2} = R(x)\{\mathbf{N_1} - \mathbf{X}\} \quad (6)$$

$$\mathbf{N_3} = R(y)\{\mathbf{N_2} - \mathbf{Y}\} \quad (7)$$

Combining them, equation (8) expresses the position of the nozzle in the build platform system ($\mathbf{N}$) from its position in the carriage system ($\mathbf{N_3}$) and from the displacements of the z, x, y machine axes.

$$\mathbf{N} = R(z) \cdot \{R^{-1}(x) \cdot [R^{-1}(y) \cdot \mathbf{N_3} + \mathbf{Y}] + \mathbf{X} - \mathbf{Z}\} \quad (8)$$

This equation can also be expressed as:

$$\mathbf{N} = \begin{pmatrix} X_N \\ Y_N \\ Z_N \end{pmatrix} = \begin{pmatrix} x + X_{N3} + \Delta X \\ y + Y_{N3} + \Delta Y \\ z + Z_{N3} + \Delta Z \end{pmatrix} \quad (9)$$

where ΔX, ΔY and ΔZ represent the position error of the nozzle caused by the geometric errors of the machine and expressed in the build platform system:

$$\Delta X = \delta_x(x) + \delta_x(y) + \delta_x(z) - y[\alpha_{xy} + \varepsilon_z(x) - \varepsilon_z(z)] + z[\alpha_{xz} + \varepsilon_y(z)] - Y_{N3}[\varepsilon_z(x) + \varepsilon_z(y) - \varepsilon_z(z)] + Z_{N3}[\varepsilon_y(x) + \varepsilon_y(y) - \varepsilon_y(z)] \quad (10)$$

$$\Delta Y = \delta_y(x) + \delta_y(y) + \delta_y(z) - x \cdot \varepsilon_z(z) + z[\varepsilon_x(z) - \alpha_{yz}] + X_{N3}[\varepsilon_z(x) + \varepsilon_z(y) - \varepsilon_z(z)] - Z_{N3}[\varepsilon_x(x) + \varepsilon_x(y) - \varepsilon_x(z)] \quad (11)$$

$$\Delta Z = \delta_z(x) + \delta_z(y) + \delta_z(z) + x \cdot \varepsilon_y(z) + y[\varepsilon_x(x) - \varepsilon_x(z)] - X_{N3}[\varepsilon_y(x) + \varepsilon_y(y) - \varepsilon_y(z)] + Y_{N3}[\varepsilon_x(x) + \varepsilon_x(y) - \varepsilon_x(z)] \quad (12)$$

3.2. Simplification of the general model

In order to apply the model stated in the previous section, it is necessary to know the error functions presented in Table 2, adapting them to the specific AM technique used (e.g., FFF in this work).

In most of the AM techniques available today, the element in charge of materialising the part geometry remains fixed to the moving part of the machine that is responsible for its displacement. Thus, in the FFF technique used in this work, the extrusion nozzle remains fixed to the head on the machine carriage. Therefore, the model previously described can be simplified by neglecting the nozzle offset with respect to the carriage reference system ($\mathbf{N_3}$).

On the other hand, although equations (10) to (12) characterise the geometric errors of the machine along the three directions of space, compensation of these errors is not always adequate since it will depend on the type of control architecture and technique used by the AM machine. In particular, regarding the FFF technique, the correction of the Z-axis (equation (12)) as a function of positions x and y may lead to the occurrence of collisions between the nozzle and the build platform or even with the material deposited on the preceding layers. This would result in damage to the system or serious defects in manufactured parts. The same phenomenon would occur when techniques other than FFF are used. Therefore, since it is desirable that the Z-correction depends only on the z-displacement, equation (12) must be simplified by eliminating the terms $\delta_z(x), \delta_z(y), \varepsilon_y(z), \varepsilon_x(x)$ and $\varepsilon_x(z)$.

To avoid an excessive degree of complexity in the determination of error functions, polynomial functions have been used, similarly to other existing works on error modelling in CNC machines (Tong *et al.*, 2003, 2008; Bochmann *et al.*, 2015; Cajal *et al.*, 2016; Majarena *et al.*, 2017; Kruth *et al.*, 1994).

Thus, displacement errors will be defined by third degree polynomials and, in the case of angular errors, by second degree polynomials without ordinate at the origin. The use of third degree polynomials for the displacement errors makes it possible to eliminate the constant squareness terms in equations (10) and (11) (Kruth *et al.*, 1994). Apart from that, the constant terms of the third degree polynomials were grouped into constant terms (i.e., ΔX_0, ΔY_0 and ΔZ_0) in each equation.

Taking all these simplifications into account, equations (10) to (12) are transformed into the following:

$$\Delta X = \delta_x(x) + \delta_x(y) + \delta_x(z) - y[\varepsilon_z(x) - \varepsilon_z(z)] + \Delta X_0 \tag{13}$$

$$\Delta Y = \delta_y(x) + \delta_y(y) + \delta_y(z) - x \cdot \varepsilon_z(z) + \Delta Y_0 \tag{14}$$

$$\Delta Z = \delta_z(z) + \Delta Z_0 \tag{15}$$

Substituting the error functions into these equations by their polynomial expressions, they will be transformed as follows:

$$\begin{aligned} \Delta X = {} & a_1^{\delta_{xx}} \cdot x + a_2^{\delta_{xx}} \cdot x^2 + a_3^{\delta_{xx}} \cdot x^3 + a_1^{\delta_{xy}} \cdot y + a_2^{\delta_{xy}} \cdot y^2 \\ & + a_3^{\delta_{xy}} \cdot y^3 + a_1^{\delta_{xz}} \cdot z + a_2^{\delta_{xz}} \cdot z^2 + a_3^{\delta_{xz}} \cdot z^3 \\ & - y \cdot \left[a_1^{\varepsilon_{zx}} \cdot x + a_2^{\varepsilon_{zx}} \cdot x^2 - a_1^{\varepsilon_{zz}} \cdot z - a_2^{\varepsilon_{zz}} \cdot z^2\right] + \Delta X_0 \end{aligned} \tag{16}$$

$$\Delta Y = a_1^{\delta_{yx}} \cdot x + a_2^{\delta_{yx}} \cdot x^2 + a_3^{\delta_{yx}} \cdot x^3 + a_1^{\delta_{yy}} \cdot y + a_2^{\delta_{yy}} \cdot y^2 + a_3^{\delta_{yy}} \cdot y^3 + a_1^{\delta_{yz}} \cdot z + a_2^{\delta_{yz}} \cdot z^2 + a_3^{\delta_{yz}} \cdot z^3 - x \cdot \left[a_1^{\varepsilon_{zz}} \cdot z + a_2^{\varepsilon_{zz}} \cdot z^2\right] + \Delta Y_0 \quad (17)$$

$$\Delta Z = a_1^{\delta_{zz}} \cdot z + a_2^{\delta_{zz}} \cdot z^2 + a_3^{\delta_{zz}} \cdot z^3 + \Delta Z_0 \quad (18)$$

where the nomenclature has been simplified by expressing the functions $\delta_i(j)$ as δ_{ij}.

On the other hand, expressions (16) to (18) can be expressed together by a single matrix expression as:

$$A \cdot m = b \quad (19)$$

where:

- b is a column vector with 3 rows containing ΔX, ΔY and ΔZ
- m is a column vector with 28 rows including the 25 different coefficients appearing in the expressions and the 3 constant terms ΔX_0, ΔY_0, ΔZ_0
- A is a matrix of 3 rows and 28 columns whose terms are the polynomial variables corresponding to each machine displacement (i.e., x, y, z) with their corresponding degree and sign.

The linear system shown in equation (19) can be solved by least squares to obtain m as follows:

$$m = (A^T \cdot A)^{-1} \cdot A^T \cdot b \quad (20)$$

where $(A^T \cdot A)^{-1} \cdot A^T$ is the pseudo-inverse of the matrix A.

Since there are 28 coefficients to be determined and only three equations for each point, the virtual points obtained from the measurement of the master artefact manufactured on the test bench shall be used. In this way, the matrix A will be transformed into the extended matrix A_n, where n represents the number of virtual points calculated (i.e., 144). Thus, the expression (20) will be transformed as:

$$m = (A_n^T \cdot A_n)^{-1} \cdot A_n^T \cdot b \quad (21)$$

In this least squares-based resolution, b is the vector of position deviations of the virtual points from their nominal values and m is the vector of the model coefficients. The use of the least squares method makes it possible to obtain the statistical parameter *p-value* associated with each coefficient of the model, which allows for optimising the model.

3.3. Model validation

In this section, the coefficients of the geometric error model for the test bench are determined from the measurement results of the master artefact manufactured in this machine. The model is then optimised and applied to the production of a new compensated artefact to test the error reduction.

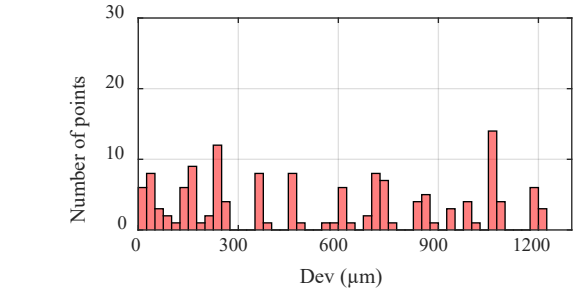

(a)

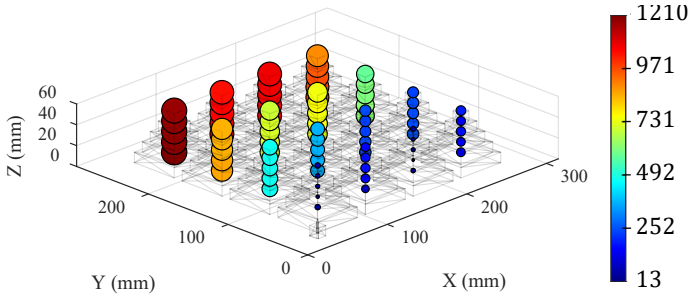

(b)

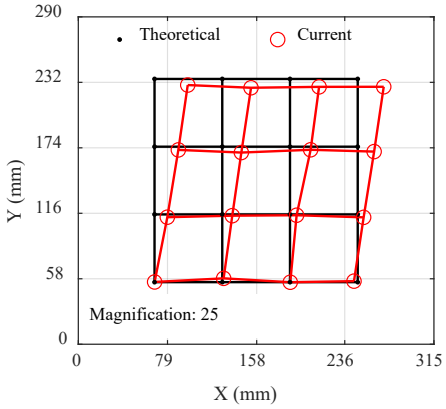

(c)

Figure 6. Measured deviations for virtual points before applying compensation: (a) histogram, (b) volumetric distribution, (c) projected deviations on the OXY plane.

Thus, Figure 6a shows the histogram of deviations detected between the real and theoretical three-dimensional distance of each of the 144 virtual points. It can be seen that the maximum deviation is 1212.4 µm. These deviations have also been plotted in Figure 6b for each step of each pyramid. There is a combined effect of the X and Y axes mainly due to a squareness error which is clearly seen in the representation of deviations in Figure 6c.

The system in equation (21) was solved by least squares using the previous deviations, obtaining $R^2 = 99.00\%$, RMSE $= 38.3$ µm and the coefficients of the error functions are shown in Table 3. Despite the high quality of the fit, it can be observed that some *p-values* associated with the coefficients are higher than 0.05. This means that they are not statistically significant and may lead to an overfitting problem. Therefore, it was decided

to solve the model again, discarding those coefficients that were low significant, except for the independent terms and for the term $a_1^{\delta_{zz}}$ due to convergence reasons.

Table 3. Coefficients obtained for the initial model ($R^2 = 99.00\%$; RMSE $= 38.3$ µm).

	Coefficients				*p-values* of the coefficients			
	a_0^*	a_1	a_2	a_3	a_0^*	a_1	a_2	a_3
δ_{xx}	6.21E-02	-5.17E-03	4.49E-05	-1.20E-07	0.53	<0.01	<0.01	<0.01
δ_{yy}	1.37E-01	-4.47E-03	2.22E-05	-5.22E-08	0.13	<0.01	0.02	0.02
δ_{zz}	4.03E-02	-5.17E-03	1.30E-04	-1.30E-06	0.23	0.25	0.43	0.49
δ_{xy}	-	2.20E-03	4.36E-05	-1.00E-07	-	0.09	<0.01	<0.01
δ_{xz}	-	6.07E-04	-1.95E-05	2.31E-07	-	0.90	0.91	0.90
δ_{yx}	-	-1.15E-03	9.54E-06	-2.35E-08	-	0.45	0.36	0.29
δ_{yz}	-	1.55E-02	-4.32E-04	3.41E-06	-	<0.01	0.01	0.07
ε_{zz}	-	8.41E-06	-1.93E-07	-	-	0.50	0.37	-
ε_{zx}	-	2.60E-05	-7.53E-08	-	-	<0.01	<0.01	-

*Values and *p-values* corresponding to $\Delta X_0, \Delta Y_0, \Delta Z_0$

This optimisation process resulted in the coefficients shown in Table 4, with $R^2 = 98.94\%$ and RMSE $= 38.8$ µm, using only 16 of the 28 coefficients in the initial model. As it can be seen, all coefficients of this model have statistical significance (i.e., *p-value* below 0.05) except for the one corresponding to ΔZ_0.

Table 4. Coefficients obtained for the optimised model ($R^2 = 98.94\%$; RMSE $= 38.8$ µm).

	Coefficients				p-values of the coefficients			
	a_0^*	a_1	a_2	a_3	a_0^*	a_1	a_2	a_3
δ_{xx}	1.64E-01	-5.41E-03	4.56E-05	-1.20E-07	0.02	<0.01	<0.01	<0.01
δ_{yy}	1.49E-01	-4.47E-03	2.22E-05	-5.22E-08	0	<0.01	0.02	0.02
δ_{zz}	9.38E-03	-1.31E-03	-	-	0.22	<0.01	-	-
δ_{xy}	-	-	5.99E-05	-1.37E-07	-	-	<0.01	<0.01
δ_{xz}	-	-	-	-	-	-	-	-
δ_{yx}	-	-	-	-	-	-	-	-
δ_{yz}	-	6.38E-03	-1.00E-04	-	-	<0.01	<0.01	-
ε_{zz}	-	-	-	-	-	-	-	-
ε_{zx}	-	2.43E-05	-7.05E-08	-	-	<0.01	<0.01	-

*Values and p-values corresponding to $\Delta X_0, \Delta Y_0, \Delta Z_0$ of the model

Once the model was optimised, a new design of the artefact was carried out by applying a compensation of the detected errors, which consisted in correcting the triangle vertices and normal vectors of the original STL file to obtain a new compensated STL. Once the new artefact was manufactured using the same parameters as in the initial process (Table 1), it was measured on the CMM and the deviations of the virtual points were obtained (Figure 7). Comparing these results with those obtained before compensation (Figure 6), a substantial improvement of the results is observed, with a maximum deviation of 300 µm, which enables to validate the developed model.

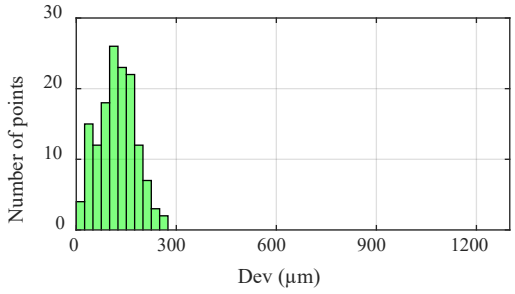

(a)

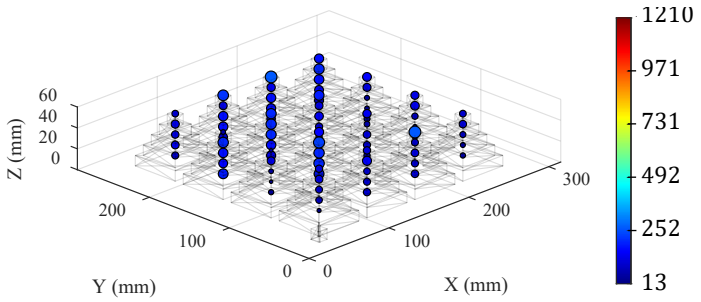

(b)

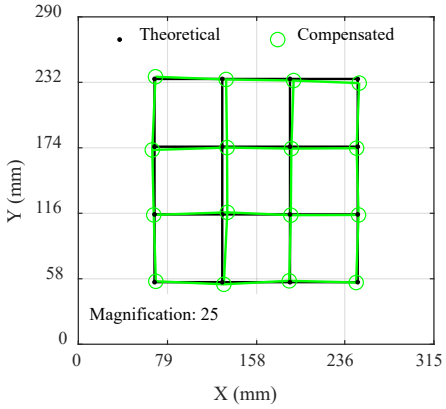

(c)

Figure 7. Measured deviations for virtual points after applying compensation: (a) histogram, (b) volumetric distribution, (c) projected deviations on the OXY plane.

4. Case study

In order to validate the developed error compensation model, it was applied to the manufacture of an example part as shown in Figure 8a. This is a template for positioning shafts in a mechanical system, in which it is essential to ensure the position of the centres as well as the diameter values of the cylindrical features (C1 to C7). Three units of the same part were manufactured in the test bench: one without geometric compensation (NC), another one including geometric compensation (GC) and a third one in which a simple dimensional correction (GDC) was added to the geometric compensation, as it will be explained in section 4.1. The same process parameters were used in all cases as for the master artefact (Table 1).

All parts were measured in the CMM without removing them from the glass of the build

platform, as in the case of the pyramid artefact (Figure 8b) and taking into account recommendations included in ISO/ASTM 52902. The alignment was performed by fixing the origin at the centre of the hole C1 and setting the direction of the X-axis between the centres C1 and C2. After the measurement process, the position deviations of the centres of the different cylindrical features C1 to C7 were analysed, both in the X and Y directions as well as in the combination of both axes (i.e., Δ_X, Δ_Y and Δ_{XY}). The results are shown in Table 5.

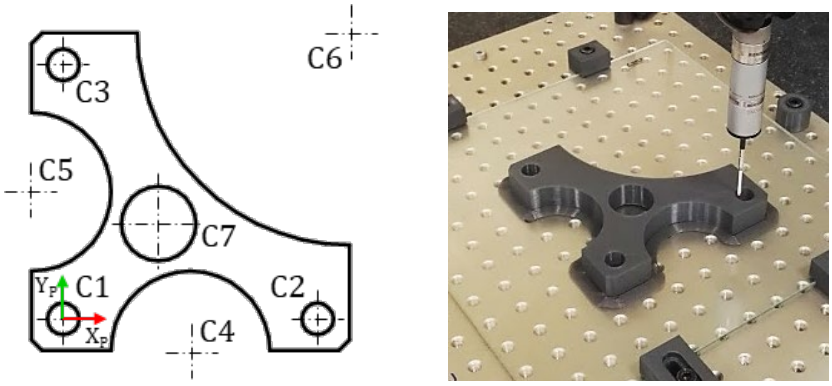

(a) (b)

Figure 8. Case study part: (a) general shape and nomenclature of cylindrical features, (b) measurement on the CMM.

Table 5. Theoretical positions and deviations measured on the part with no geometric compensation (NC), with geometric compensation (GC) and with both geometric and dimensional compensation (GDC).

	Position		NC			GC			GDC		
ID	X (mm)	Y (mm)	Δ_X (µm)	Δ_Y (µm)	Δ_{XY} (µm)	Δ_X (µm)	Δ_Y (µm)	Δ_{XY} (µm)	Δ_X (µm)	Δ_Y (µm)	Δ_{XY} (µm)
C2	120	0	-70	52	87	-53	48	72	-66	-13	67
C3	0	120	947	-319	999	25	-204	206	128	-144	192
C4	60	-15	-35	129	134	-84	36	91	-26	43	50
C5	-15	60	560	-60	563	184	-78	199	33	-177	181
C6	135	135	255	-1004	1035	332	-128	355	191	-107	219
C7	45	45	346	-138	372	-7	-159	159	55	-67	87

The combined deviations (Δ_{XY}) are shown in Figure 9. As it can be seen, the applied geometric compensation (GC) enables to substantially reduce this type of deviations below 200 µm in almost all cases, which is in accordance with the improvement achieved in the compensated master artefact (Figure 7a). In the particular case of C6, with a higher deviation (355 µm), the position of the centre was obtained from the measurement of only one quarter of the cylindrical surface, which may have affected the accuracy of the result and therefore does not constitute a sufficiently reliable metrological result. In any case, there is a great improvement over the part without compensation (NC).

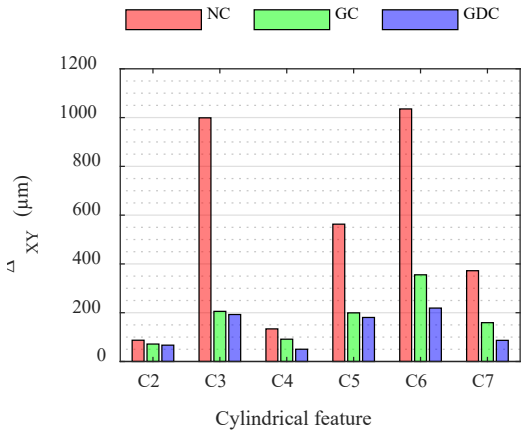

Figure 9. Combined deviations (Δ_{XY}) measured on the part with no geometric compensation (NC), with geometric compensation (GC) and with both geometric and dimensional compensation (GDC).

Table 6. Reference values and diameter deviations measured on the part with no geometric compensation (NC), with geometric compensation (GC) and with both geometric and dimensional compensation (GDC).

	Diameter	NC		GC		GDC	
	D	Δ_D		Δ_D		Δ_D	
ID	(mm)	(µm)	(%)	(µm)	(%)	(µm)	(%)
C1	15	-286	-1.9	-274	-1.8	-119	-0.8
C2	15	-353	-2.4	-319	-2.1	-138	-0.9
C3	15	-361	-2.4	-315	-2.1	-178	-1.2
C4	75	-238	-0.3	-44	-0.1	19	0.0
C5	75	-248	-0.3	-171	-0.2	77	0.1
C6	200	-1573	-0.8	235	0.1	476	0.2
C7	35	-248	-0.7	-248	-0.7	-43	-0.1

On the other hand, the diameter deviations of the cylindrical features of the part were also determined as shown in Table 6. Moreover, Figure 10 shows the percentage deviations of the diameter from the theoretical value.

It can be observed that the geometric compensation model (GC) does not substantially improve the dimensional errors of the cylindrical features of the part. This is because the measurements were obtained by using the actual points probed on the part surfaces which are clearly affected by the errors associated with the material and process.

Therefore, it can be stated that the improvement precision limit achieved in geometrically compensated parts is related to the persistence of errors associated with the AM material and process, which are not related to the geometric errors of the machine and which are not included in the developed model.

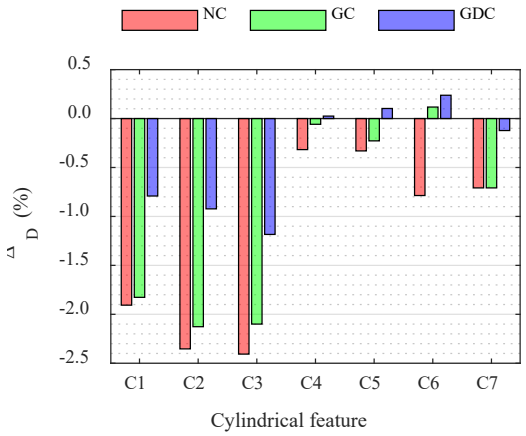

Figure 10. Diameter deviations (%) measured on the part without geometric compensation (NC), with geometric compensation (GC) and with both geometric and dimensional compensation (GDC).

4.1. Dimensional correction of the example part

The study of AM process and material-related parameters affecting part accuracy depends on the specific characteristics of the process and material under consideration. For example, in the case of FFF, some of the most influential parameters could be: layer thickness, part orientation, infill percentage, printing speed, printing temperature, etc. (Elkaseer *et al.*, 2020 and Sood *et al.*, 2009). In any case, the development of a compensation model that takes all these parameters into account requires a complex experimental study and a detailed analysis that is not covered in this paper, which is mainly focused on machine errors compensation.

Despite these circumstances, a brief study of dimensional errors has been carried out in order to improve the results achieved after the application of the geometric error compensation model. For this purpose, some dimensions of both the artefact and the example part were analysed.

In the case of the GC master artefact, distances between the opposite vertical faces on each pyramid step (160 in total) were measured. A negative average distance deviation of −162 µm (Figure 11) was observed from the theoretical ones. Since the GC artefact is not affected by the geometric machine errors, deviations could be mainly due to both process and material-related errors.

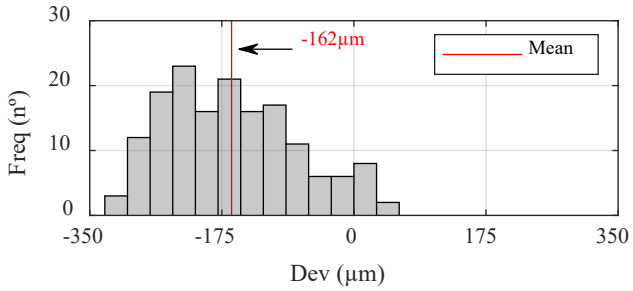

Figure 11. Histogram of distance deviations between parallel vertical planes of the master artefact pyramids with geometric compensation (GC).

Although it can be observed in Figure 11 that there exists a certain dispersion of deviations, half of the average value (i.e., −81 µm) could be used as a first approximation

to compensate for the overall part shrinkage, assuming an isotropic behaviour in the XY plane. Despite this is not always true (e.g., in the case of using various infill densities), it was decided to check whether the part dimensional improvement was significant or not. For this purpose, the correction value (i.e., −81 μm) was input to the *Ultimaker Cura* through the *Horizontal expansion* parameter, which is intended to compensate for dimensional inaccuracies of the AM process, so that a positive value will reduce the size of cavities whereas a negative value will increase them. In this case, the dimensional correction was applied to the GC test part and a new part was manufactured which was so-called the *geometrical and dimensional compensated part* (i.e., GDC part).

Figure 9 shows a low significant improvement in the position of the GDC part centres of the cylindrical features with respect to the GC part. On the contrary, Figure 10 shows a substantial improvement in the diameters of these cylinders.

Therefore, it can be stated that the application of this dimensional correction provides a dimensional improvement in the cylindrical characteristics with no detriment to the corrections made by the geometric compensation model. Consequently, the combined application of both corrections ensures that the example part meets the functional requirements.

5. Conclusions

In the present work, a model was developed for off-line compensation of geometric errors in AM machines by isolating them from process and material-related errors. This is an advantage compared to most of the studies carried out so far concerning geometric error compensation, which do not consider the separation between the three error sources and thus, they do not enable to reproduce same results on different machines. Although the model was tested on a specific FFF test bench and some simplifications were applied accordingly, the methodology is extensible to any other type of AM machine.

To develop the model, a specific master artefact was designed, manufactured and later measured on a CMM. The metrological information of the artefact was based on the calculation of virtual points, which are independent of dimensional inaccuracies, making possible to isolate the machine geometric errors from the other error sources.

After some adjustments and simplifications, the model effectiveness was tested by measuring a new artefact that was constructed including compensation for the geometric errors previously detected. Residual errors below 300 μm were observed in the position of the virtual points, which in this case were mainly derived from the material and process errors. Similarly, the geometric error model was applied to manufacture a compensated example part showing position deviations of its functional characteristics (i.e., centres of the cylindrical surfaces) below 200 μm, roughly matching the results obtained for the master artefact. Despite this, the dimensional values of the functional characteristics (i.e., diameters of the cylindrical surfaces) did not improve substantially after the application of the error model, with maximum deviations of around 2% from the theoretical value. A simple way to compensate for this dimensional deviation was to use the *Horizontal expansion* factor available in the 3D printing software. In this way, it was possible to reduce the maximum dimensional errors to 1% without altering the position errors met by applying only the geometric compensation. Consequently, the combined application of both corrections allowed the functional requirements of the example part to be fulfilled.

The study carried out demonstrates the effectiveness of the model developed for improving the geometric precision of parts manufactured on AM machines, fundamentally those related to the squareness and positioning of machine axes. The errors

that persist in the part derive from the material and process and, therefore, they are independent of the AM machine on which it is produced. The compensation for these material and process errors requires a detailed analysis of the influencing parameters, which will be the subject of future research. Based on this analysis, a predictive model that includes the three error sources will be developed to compensate for deviations on the deposited layers, thus improving the overall geometric part accuracy. The adjustment of the model will be carried out by comparing the predicted errors with those detected on each layer by means of a non-contact digitizing system. In this way, a digital twin will be obtained to optimise the process and system performance of AM.

Acknowledgements

This work was supported by the Spanish Ministry of Science, Innovation and Universities and by FEDER (DPI2017-83068-P).

References

Abdelrahman, M., Reutzel, E.W., Nassar, A.R. and Starr, T.L. (2017), "Flaw detection in powder bed fusion using optical imaging", Additive Manufacturing, Vol. 15, pp.1–11. https://doi.org/10.1016/j.addma.2017.02.001.

ASME B5.54-1992 (2005), Methods for Performance Evaluation of Computer Numerically Controlled Machining Centers, American Society of Mechanical Engineers (ASME).

Beltrán, N., Álvarez, B.J., Blanco, D., Peña, F. and Fernández, P. (2021), "A design for additive manufacturing strategy for dimensional and geometrical quality improvement of PolyJet-manufactured glossy cylindrical features", Polymers, Vol. 13, No. 7, pp.1132. https://doi.org/10.3390/polym13071132.

Bochmann, L., Bayley, C., Helu, M., Transchel, R., Wegener, K. and Dornfeld, D. (2015), "Understanding error generation in fused deposition modelling", Surface Topography: Metrology and Properties, Vol. 3 No. 1, pp.014002. https://doi.org/10.1088/2051-672X/3/1/014002.

Bringmann, B. and Knapp, W. (2006), "Model-based 'chase-the-ball' calibration of a 5-axes machining center", CIRP annals, Vol. 55, No. 1, pp.531–534. https://doi.org/10.1016/S0007-8506(07)60475-2.

Cajal, C., Santolaria, J., Samper, D. and Velazquez, J. (2016), "Efficient volumetric error compensation technique for additive manufacturing machines", Rapid Prototyping J., Vol. 22 No. 1, pp.2–19. https://doi.org/10.1108/RPJ-05-2014-0061.

Campbell, I., Bourell, D. and Gibson I. (2012), "Additive manufacturing: rapid prototyping comes of age", Rapid Prototyping J., Vol. 18 No. 4, pp.255–258. https://doi.org/10.1108/13552541211231563.

Carmignato, S., De Chiffre, L., Bosse, H., Leach, R.K., Balsamo, A. and Estler, W.T. (2020), "Dimensional artefacts to achieve metrological traceability in advanced manufacturing", CIRP annals, Vol. 69, No. 2, pp.693–716. https://doi.org/10.1016/j.cirp.2020.05.009.

Deng, M., Li, H., Xiang, S., Liu, P., Feng, X., Du, Z., and Yang, J. (2020), "Geometric errors identification considering rigid-body motion constraint for rotary axis of multi-axis machine tool using a tracking interferometer", International Journal of Machine Tools and Manufacture, Vol. 158, pp.103625.

https://doi.org/10.1016/j.ijmachtools.2020.103625.

Elkaseer, A., Schneider, S. and Scholz, S.G. (2020), "Experiment-based process modeling and optimization for high-quality and resource-efficient FFF 3D printing", Appl. Sci-Bas., Vol. 10 No. 8, pp.2899. https://doi.org/10.3390/app10082899.

Fang, X., Du, J., Wei, Z., He, P., Bai, H., Wang, X. and Lu, B. (2017), "An investigation on effects of process parameters in fused-coating based metal additive manufacturing", Journal of Manufacturing Processes, Vol. 28, pp.383–389. https://doi.org/10.1016/j.jmapro.2017.01.008.

Fico, D., Rizzo, D., Casciaro, R. and Esposito Corcione, C. (2022), "A review of polymer-based materials for Fused Filament Fabrication (FFF): Focus on sustainability and recycled materials", Polymers, Vol. 14 No. 3, pp.465. https://doi.org/10.3390/polym14030465.

Foster, B.K., Reutzel, E.W., Nassar, A.R., Hall, B.T., Brown, S.W. and Dickman, C.J. (2015), "Optical, layerwise monitoring of powder bed fusion", in Proceedings of the 21th Annual International Solid Freeform Fabrication Symposium, University of Texas at Austin, pp.295–307. https://hdl.handle.net/2152/89328.

Haghshenas Gorgani, H., Korani, H., Jahedan, R. and Shabani, S. (2021), "A Nonlinear Error Compensator for FDM 3D Printed Part Dimensions Using a Hybrid Algorithm Based on GMDH Neural Network", Journal of Computational Applied Mechanics, Vol. 52 No. 3, pp.451–477. https:\\doi.org/10.22059/JCAMECH.2021.325325.628.

Hartmann, C., Lechner, P., Himmel, B., Krieger, Y., Lueth, T.C. and Volk, W. (2019), "Compensation for Geometrical Deviations in Additive Manufacturing", Technologies, Vol. 7 No. 4, pp.83. https://doi.org/10.3390/technologies7040083.

Iñigo, B., Colinas-Armijo, N., de Lacalle, L.N.L. and Aguirre, G. (2021), "Digital twin-based analysis of volumetric error mapping procedures", Precision Engineering, Vol. 72, pp.823–836. https://doi.org/10.1016/j.precisioneng.2021.07.017.

ISO/ASTM 52902:2019 (2019), Additive manufacturing – Test artifacts – Geometric capability assessment of additive manufacturing systems, International Organization for Standardization (ISO).

ISO 17296-2:2015 (2015), Additive manufacturing – General principles – Part 2: Overview of process categories and feedstock, International Organization for Standardization (ISO).

ISO 10360-2:2009 (2009), Geometrical product specifications (GPS) – Acceptance and reverification tests for coordinate measuring machines (CMM) – Part 2: CMMs used for measuring linear dimensions, International Organization for Standardization (ISO).

ISO 230-1:2012 (2012), Test code for machine tools – Part 1: Geometric accuracy of machines operating under no-load or quasi-static conditions, International Organization for Standardization (ISO).

Javaid, M. and Haleem, A. (2018), "Additive manufacturing applications in medical cases: A literature based review", Alexandria Journal of Medicine, Vol. 54 No. 4, pp.411–422. https://doi.org/10.1007/s00170-017-1385-8.

Kadir, A. A., Xu, X. and Hämmerle, E. (2011), "Virtual machine tools and virtual machining—a technological review", Robotics and computer-integrated manufacturing, Vol. 27, No. 3, pp.494–508. https://doi.org/10.1016/j.rcim.2010.10.003.

Klassen, A., Forster, V.E., Juechter, V. and Körner, C. (2017), "Numerical simulation of multi-component evaporation during selective electron beam melting of TiAl", Journal of Materials Processing Technology, Vol. 247, pp.280–288. https://doi.org/10.1016/j.jmatprotec.2017.04.016.

Kruth, J.P., Vanherck, P. and de Jonge, L. (1994), "Self-calibration method and software error correction for three-dimensional coordinate measuring machines using artefact measurements", Measurement, Vol. 14 No. 2, pp.157–167. https://doi.org/10.1016/0263-2241(94)90024-8.

Leng, J., Wang, D., Shen, W., Li, X., Liu, Q. and Chen, X. (2021), "Digital twins-based smart manufacturing system design in Industry 4.0: A review", Journal of manufacturing systems, Vol. 60, pp.119–137. https://doi.org/10.1016/j.jmsy.2021.05.011.

Lyu, J. and Manoochehri, S. (2019), "Error modeling and compensation for FDM machines", Rapid Prototyping Journal, Vol. 25, No. 10, pp.1565–1574. https://doi.org/10.1108/RPJ-04-2017-0068.

Majarena, A.C., Aguilar, J.J. and Santolaria, J. (2017), "Development of an error compensation case study for 3D printers", Procedia Manufacturing, Vol. 13, pp.864–871. https://doi.org/10.1016/j.promfg.2017.09.145.

Mohamed, O.A., Masood, S.H. and Bhowmik, J.L. (2021), "Modeling, analysis, and optimization of dimensional accuracy of FDM-fabricated parts using definitive screening design and deep learning feedforward artificial neural network", Advances in Manufacturing, Vol. 9 No. 1, pp.115–129. https://doi.org/10.1007/s40436-020-00336-9.

Moretti, M., Rossi, A. and Senin, N. (2021), "In-process monitoring of part geometry in fused filament fabrication using computer vision and digital twins", Addit. Manuf., Vol. 37, pp.101609. https://doi.org/10.1016/j.addma.2020.101609.

Moroni, G., Petrò, S. and Shao, H. (2020), "On standardization efforts for additive manufacturing", in Wang, L., Majstorovic, V.D., Mourtzis, D., Carpanzano, E., Moroni, G. & Galantucci, L.M. (Ed.s), Proceedings of 5th International Conference on the Industry 4.0 Model for Advanced Manufacturing, Springer, Belgrade, pp.156–172. https://doi.org/10.1007/978-3-030-46212-3_11.

Moroni, G., Syam, W.P. and Petro, S. (2014), "Towards early estimation of part accuracy in additive manufacturing", Procedia Cirp, Vol. 21, pp. 300–305. https://doi.org/10.1016/j.procir.2014.03.194.

Najmon, J.C., Raeisi, S. and Tovar, A. (2019), "Review of additive manufacturing technologies and applications in the aerospace industry", in Froes F. & Boyer R. (Ed.s), Additive manufacturing for the aerospace industry, Elsevier, Amsterdam, pp.7–31. https://doi.org/10.1016/B978-0-12-814062-8.00002-9.

Oliveira, J.P., LaLonde, A.D. and Ma, J. (2020), "Processing parameters in laser powder bed fusion metal additive manufacturing", Materials & Design, Vol. 193, pp.108762. https://doi.org/10.1016/j.matdes.2020.108762.

Omairi, A. and Ismail, Z.H. (2021), "Towards machine learning for error compensation in additive manufacturing", Applied Sciences, Vol. 11 No. 5, pp.2375. https://doi.org/10.3390/app11052375.

Peña, F., Fernández, C., Valiño, G., Álvarez, B.J. and Rico, J.C. (2021), "Design and

Construction of a Test Bench for the Manufacture and On-machine Non-contact Inspection of Parts Obtained by Fused Filament Fabrication", IOP Conf. Ser.: Mater. Sci. Eng., Vol. 1193, pp.012090. https://doi.org/10.1088/1757-899X/1193/1/012090.

Schellekens, P.H.J., Spaan, H.A.M., Soons, J.A., Trapet, E., Loock, V., Dooms, J., Ruiter, H. and Maisch, M. (1993), "Development of methods for numerical error correction of machine tools", in Ikawa, N., Shimada, S., Moriwaki, T., Mckeown, P.A. & Spragg, R.C. (Ed.s), International Progress in Precision Engineering: Proceedings of the 7th International Precision Engineering Seminar, Stoneham, Massachusetts: Butterworth-Heinemann, Kobe, pp.212–223. https://doi.org/10.1016/B978-0-7506-9484-1.50025-7.

Schwenke, H., Knapp, W., Haitjema, H., Weckenmann, A., Schmitt, R. and Delbressine, F. (2008), "Geometric error measurement and compensation of machines–an update", CIRP annals, Vol. 57 No. 2, pp.660–675. https://doi.org/10.1016/j.cirp.2008.09.008.

Shanmugam, V., Pavan, M.V., Babu, K. and Karnan, B. (2021), "Fused deposition modeling based polymeric materials and their performance: A review", Polymer Composites, Vol. 42 No. 11, pp.5656–5677. https://doi.org/10.1002/pc.26275.

Song, S., Wang, A., Huang, Q. and Tsung, F. (2014), "Shape deviation modeling for fused deposition modeling processes", in IEEE (Ed.s), Proceedings of the 2014 IEEE International Conference on Automation Science and Engineering (CASE), IEEE, Taipei, pp.758–763. https://doi.org/10.1109/CoASE.2014.6899411.

Sood, A.K., Ohdar, R.K. and Mahapatra, S.S. (2009), "Improving dimensional accuracy of fused deposition modelling processed part using grey Taguchi method", Mater. Des., Vol. 30, No. 10, pp.4243–4252. https://doi.org/10.1016/j.matdes.2009.04.030.

Sutton, A.T., Kriewall, C.S., Leu, M.C. and Newkirk, J. W. (2016), "Powders for Additive Manufacturing Process: Characterization Techniques and Effects on Part Properties", in Proceedings of the 21th Annual International Solid Freeform Fabrication Symposium, University of Texas at Austin, pp.1004–1030. https://hdl.handle.net/2152/89651.

Tao F., Qi Q., Wang L. and Nee, A.Y.C. (2019), "Digital twins and cyber–physical systems toward smart manufacturing and industry 4.0: Correlation and comparison", Engineering, Vol. 5, No. 4, pp.653–661. https://doi.org/10.1016/j.eng.2019.01.014.

Tong, K., Joshi, S. and Lehtihet, E.A. (2008), "Error compensation for fused deposition modeling (FDM) machine by correcting slice files", Rapid Prototyping J., Vol. 14 No. 1, pp.4–14. http://dx.doi.org/10.1108/13552540810841517.

Tong K., Lehtihet E.A. and Sanjay J. (2004), "Software compensation of rapid prototyping machines", Precision Engineering, Vol. 28, No. 3, pp.280–292, https://doi.org/10.1016/j.precisioneng.2003.11.003.

Tong, K., Lehtihet, E.A. and Joshi, S. (2003), "Parametric error modeling and software error compensation for rapid prototyping", Rapid Prototyping J., Vol. 9 No. 5, pp.301–313. https://doi.org/10.1108/13552540310502202.

Vanaei, H., Shirinbayan, M., Deligant, M., Raissi, K., Fitoussi, J., Khelladi, S. and Tcharkhtchi, A. (2020), "Influence of process parameters on thermal and mechanical properties of polylactic acid fabricated by fused filament fabrication", Polymer Engineering & Science, Vol. 60 No. 8, pp.1822–1831. https://doi.org/10.1002/pen.25419.

Vock, S., Klöden, B., Kirchner, A., Weißgärber, T. and Kieback, B. (2019), "Powders for powder bed fusion: a review", Progress in Additive Manufacturing, Vol. 4 No. 4, pp.383–397. https://doi.org/10.1007/s40964-019-00078-6.

Wang C.S. and Chang, T.R. (2008), "Re-triangulation in STL meshes for rapid prototyping and manufacture", The International Journal of Advanced Manufacturing Technology, Vol. 37, No. 7, pp.770–781. https://doi.org/10.1007/s00170-007-1009-9.

Yuasa, K., Tagami, M., Yonehara, M., Ikeshoji, T.T., Takeshita, K., Aoki, H. and Kyogoku, H. (2021), "Influences of powder characteristics and recoating conditions on surface morphology of powder bed in metal additive manufacturing", The International Journal of Advanced Manufacturing Technology, Vol. 115 No. 11, pp.3919–3932. https://doi.org/10.1007/s00170-021-07359-x.

Zhang, G. (2012), "Error compensation of coordinate measuring machines", Hocken, R.J. and Pereira, P.H. (Ed.), Coordinate Measuring Machines and Systems, CRC Press, Boca Raton, FL, pp.319–359.